

Squeezing Mismatch in the Inverse-Squeezing Kennedy Receiver for Binary Displaced Squeezed-State Discrimination

Enhao Bai

*Information Support Force Engineering University, Wuhan 430035, China and
Guangxi Key Laboratory of Multimedia Communications and Network Technology, Guangxi University, Nanning 530006, China*

Jian Peng, Tianyi Wu, and Chen Dong*

Information Support Force Engineering University, Wuhan 430035, China

Fengkai Sun and Zhenrong Zhang[†]

Guangxi Key Laboratory of Multimedia Communications and Network Technology, Guangxi University, Nanning 530006, China

Chun Zhou

Henan Key Laboratory of Quantum Information and Cryptography, SSF IEU, Zhengzhou 450001, China

Yaping Li

Wuhan Maritime Communication Research Institute, Wuhan 430035, China

(Dated: March 25, 2026)

We analyze inverse-squeezing mismatch in the IS-Kennedy receiver for binary displaced squeezed vacuum state discrimination. Mismatch is shown to be equivalent to a residual squeezing after nulling, which modifies the output photon-number statistics and makes the optimal maximum-a-posteriori (MAP) rule generally non-single-threshold. We find that the receiver is much more sensitive to phase mismatch than to amplitude mismatch. Under amplitude-only mismatch, the saturation error with finite-resolution photon-number-resolving detection exhibits a parity-step scaling, decreasing only when the detector resolution crosses even-photon thresholds. These results clarify the physical origin of mismatch-induced degradation and identify phase locking as the key requirement for practical implementations.

I. INTRODUCTION

Quantum receivers can surpass the standard quantum limit (SQL) in binary optical-state discrimination by exploiting the structure of the signal set and appropriate measurement design. Beyond the extensively studied coherent-state case, displaced squeezed vacuum states provide an important nonclassical modulation format, since squeezing can improve discrimination performance when properly matched to the receiver [1]. For binary phase-shift-keyed displaced squeezed states (S-BPSK), the optimal squeezing fraction minimizes both the Helstrom bound and the SQL, making this alphabet a natural platform for studying squeezing-enhanced quantum communication [2–4].

Recently, an inverse-squeezing Kennedy (IS-Kennedy) receiver was proposed for S-BPSK discrimination [1]. In the ideal case, the receiver first performs Kennedy nulling and then applies an inverse-squeezing operation, thereby mapping the squeezed on-off-keyed output into a coherent-state on-off-keyed alphabet before photon counting. This transformation converts the squeezing resource into an effective coherent-energy gain and allows the receiver to outperform the S-BPSK SQL [3] over a broad signal range.

In practice, however, the inverse-squeezing stage is highly sensitive to implementation imperfections. Deviations in the squeezing magnitude or phase may arise from optical loss, pump fluctuations, and phase-locking errors [5, 6], and even small mismatch can qualitatively change the receiver output statistics. This practical issue is particularly important because the performance advantage of the IS-Kennedy receiver relies on accurate cancellation of the input squeezing. In this letter, we investigate inverse-squeezing mismatch in the IS-Kennedy receiver for S-BPSK discrimination. We show that mismatch is equivalent to a residual squeezing after nulling, which makes the optimal maximum-a-posteriori (MAP) decision generally non-single-threshold. We further show that the receiver is much more sensitive to phase mismatch than to amplitude mismatch, and that under amplitude-only mismatch the saturation error with finite-resolution PNR detection exhibits a parity-step scaling. These results clarify the physical origin of mismatch-induced degradation and identify the phase-locking accuracy required for practical implementations of inverse-squeezing receivers.

* dongchengfd@163.com

[†] zxr76@gxu.edu.cn

II. RECEIVER MODELING

Here, let us consider the modeling of the Inverse-squeezing Kennedy receiver [1]. Fig. 1 shows the schematic of the inverse-squeezing Kennedy receiver.

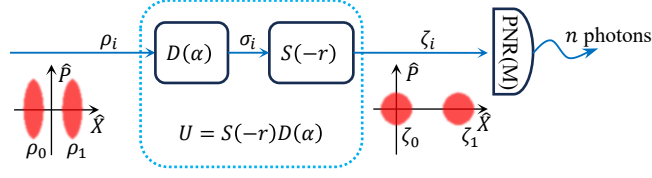


FIG. 1. The schematic of the inverse-squeezing Kennedy receiver.

The S-BPSK signals to be discriminated are defined as [3]:

$$\begin{aligned} \text{hypothes '0'} : |\psi_0\rangle &= D(-\alpha)S(r)|0\rangle \sim \rho_0, \\ \text{hypothes '1'} : |\psi_1\rangle &= D(+\alpha)S(r)|0\rangle \sim \rho_1. \end{aligned} \quad (1)$$

Without loss of generality, α is chosen to be real, and the mean photon numbers of the signals are $N = |\alpha|^2 + \sinh^2(r)$. Throughout this letter, a *priori* probability π_i of these displaced squeezed vacuum states are assumed to be equal for 2, i.e. $\pi_i = \frac{1}{2}$.

Reference [3] defines the squeezing fraction β (the share of the total energy stored in squeezing) to quantify the advantage of S-BPSK:

$$\beta \triangleq \frac{\sinh^2(r)}{N}. \quad (2)$$

In addition, under ideal condition, the optimal squeezing fraction is $\beta_{\text{opt}} = \frac{N}{2N+1}$, at which point Helstrom bound and SQL of S-BPSK are minimized [3]. In this letter, all S-BPSK employ the optimal squeezing fraction β_{opt} :

$$\alpha = \sqrt{N(1 - \beta_{\text{opt}})}, \quad r = \sinh^{-1} \sqrt{N\beta_{\text{opt}}}, \quad \alpha e^r = \sqrt{N(N+1)} \quad (3)$$

A. Receiver under ideal condition

Under ideal condition, firstly, the received signal interferes with a local oscillator (LO) on a highly transmissive beam splitter ($\tau \rightarrow 1$) to perform the Kennedy nulling displacement $D(\alpha)$. Consequently, the S-BPSK alphabet is mapped to a squeezed OOK (S-OOK) alphabet σ_i :

$$\sigma_i \sim D(\alpha)|\psi_i\rangle = \begin{cases} S(r)|0\rangle, & i = 0, \\ D(2\alpha)S(r)|0\rangle, & i = 1. \end{cases} \quad (4)$$

Subsequently, σ_i passes through the IS module $S(-r)$, mapping the S-OOK alphabet to a coherent-state OOK (C-OOK) alphabet ζ_i :

$$\zeta_i = S(-r)\sigma_i S^\dagger(-r) \sim \begin{cases} S(-r)S(r)|0\rangle = |0\rangle, & i = 0, \\ S(-r)D(2\alpha)S(r)|0\rangle = D(2\alpha e^r)|0\rangle = |2\gamma\rangle. & i = 1. \end{cases} \quad (5)$$

In the general case, $\gamma = \alpha \cosh r + \alpha^* \sinh r$. In this letter $\alpha \in \mathbb{R}_+$, so $\gamma = \alpha e^r$. Therefore, we define:

$$\gamma \triangleq \alpha e^r, \quad N_{\text{eff}} \triangleq |\gamma|^2 = |\alpha|^2 e^{2r}. \quad (6)$$

Next, PNR detection is performed on ζ_i , yielding an output photon number n . The positive operator-valued measure (POVM) for an ideal PNR detector with resolution M , denoted as $\text{PNR}(M)$, is given by:

$$\Pi_n^{(M)} = \begin{cases} \Pi_n, & n = 0, 1, \dots, M-1 \\ \mathbb{I} - \sum_{k=0}^{M-1} \Pi_k, & n = M \end{cases} \quad (7)$$

where $\Pi_n = |n\rangle\langle n|$, $n = 0, 1, 2, \dots$ and \mathbb{I} is the identity matrix in the Fock representation.

Therefore, the probability of detecting n photons given hypotheses ' i ' is:

$$P(n|i) = \text{Tr} \left\{ \zeta \cdot \Pi_n^{(M)} \right\} = \begin{cases} \text{Poiss}(n; \mu_i), & n = 0, 1, \dots, M-1 \\ 1 - \sum_{k=0}^{M-1} \text{Poiss}(k; \mu_i), & n = M \end{cases} \quad (8)$$

where $\text{Poiss}(n; \mu) = e^{-\mu} \frac{\mu^n}{n!}$; $\mu_0 = 0$ and $\mu_1 = 4N_{\text{eff}}$ are the mean photon number of ζ_0 and ζ_1 , respectively. Then, the *posterior* probabilities are given by:

$$P(i|n) = \frac{\pi_i P(n|i)}{\sum_k \pi_k P(n|k)} = \frac{P(n|i)}{\sum_k P(n|k)} \quad (9)$$

The MAP decision rule is defined as:

$$\hat{i}(n) = \begin{cases} 1, & P(i=1|n) \geq P(i=0|n), \\ 0, & \text{otherwise.} \end{cases} \quad (10)$$

where \hat{i} is the decision of IS-Kennedy receiver. When the likelihood function $L(n) = \ln \frac{P(n|i=0)}{P(n|i=1)}$ is monotonic, the MAP decision is equivalent to a single-threshold decision[1], with the optimal threshold denoted as n_{th}^* . In addition, under ideal conditions, the optimal threshold is 1, which means that PNR detector does not provide a performance advantage over SPD in this case [1]. So the error probability of IS-Kennedy is given by:

$$\begin{aligned} P_{\text{err}}^{\text{ISK, ideal}} &= \frac{1}{2} (P_{\text{FA}} + P_{\text{Mi}}) = \frac{1}{2} [P(n \geq n_{\text{th}}^* | i=0) + P(n < n_{\text{th}}^* | i=1)] \\ &= P_{\text{err}}^{\text{K, ideal}}(N_{\text{eff}}) = \frac{1}{2} \exp[-4N(N+1)], \end{aligned} \quad (11)$$

where P_{FA} and P_{Mi} are the false alarm probability (deciding 1 when 0 is sent) and the miss probability (deciding 0 when 1 is sent), respectively, and $P_{\text{err}}^{\text{K, ideal}}$ is the ideal probability of the Kennedy receiver [7]. From this, it can be seen that the IS-Kennedy converts the squeezing resources of S-BPSK signals into higher coherent energy advantage ($N \rightarrow N_{\text{eff}} = N(N+1)$) through the IS module, thereby achieving a lower error probability. Compared to quantum receiver for coherent state discrimination, the energy gain brought by the IS-Kennedy is:

$$G = 10 \cdot \log_{10} \left(\frac{N_{\text{eff}}}{N} \right) = 10 \cdot \log_{10} (N+1) \text{ (dB)} \quad (12)$$

B. Receiver under squeezing mismatch condition

In practical experimental setups, deviations between the receiver's squeezing parameters and the input signal are inevitable due to factors such as optical loss, pump fluctuation, and phase locking errors. This phenomenon is referred to as squeezing mismatch (SM). Without loss of generality, we adopt a simplified model where the transmitter performs perfect squeezing and the optical path is lossless, attributing all squeezing adaptation errors solely to the IS module. Let the squeezing parameter applied by the IS module be denoted as:

$$z_s = (-r + \Delta r) e^{j\Delta\theta}, \quad j = \sqrt{-1}, \quad (13)$$

where Δr represents the magnitude mismatch and $\Delta\theta$ represents the phase mismatch. Under ideal conditions, $\Delta r = \Delta\theta = 0$.

Under mismatch conditions, the overall transformation of the receiver is given by:

$$\zeta_i^{\text{sm}} \sim S(z_s) D(\alpha) |\psi_i\rangle = \begin{cases} S_{\text{tot}} |0\rangle, & i = 0, \\ S_{\text{tot}} |2\gamma\rangle, & i = 1. \end{cases} \quad (14)$$

Here, the composite squeezing operator is defined as $S_{\text{tot}} \triangleq S(z_s) S(r)$, which reduces to the identity operator $S_{\text{tot}} = \mathbb{I}$ in the ideal case. Thus, the essence of the mismatch is encapsulated within S_{tot} .

Using the single-mode Gaussian operator decomposition, this operator can always be expressed as:

$$S_{\text{tot}} = R(\vartheta) S(z_m), \quad (15)$$

where $R(\vartheta) = \exp(-j\vartheta a^\dagger a)$ is a phase rotation, and $S(z_m)$ represents the equivalent residual squeezing with parameter $z_m = r_m e^{j\theta_m}$. Since $R(\vartheta)$ contributes only a phase factor in the Fock basis and does not alter the photon number distribution, the impact of mismatch on PNR statistics for a given energy N is determined solely by the residual squeezing parameters (r_m, θ_m) .

Next, we determine (r_m, θ_m) using the Bogoliubov transformation. Letting $r_s \triangleq -r + \Delta r$ and $\theta_s \triangleq \Delta\theta$, the coefficients for the transformation $S_{\text{tot}}^\dagger a S_{\text{tot}} = xa + ya^\dagger$ are derived as:

$$x = \cosh(r_s) \cosh r + e^{j\theta_s} \sinh(r_s) \sinh r, \quad y = -\cosh(r_s) \sinh r - e^{j\theta_s} \sinh(r_s) \cosh r, \quad (16)$$

satisfying the unitarity condition $|x|^2 - |y|^2 = 1$. Consequently, we obtain:

$$r_m = \text{arcsinh}(|y|), \quad \vartheta = -\arg(x), \quad \theta_m = \arg(-y) - \arg(x). \quad (17)$$

In practical scenarios characterized by small mismatches ($\Delta r \ll 1$, $|\Delta\theta| \ll 1$) [5, 6], a first-order approximation yields:

$$y \approx -\Delta r + j \frac{\Delta\theta}{2} \sinh(2r), \quad (18)$$

which leads to:

$$\begin{aligned} r_m &\approx \sqrt{(\Delta r)^2 + \left(\frac{\Delta\theta}{2} \sinh 2r\right)^2}, \\ \theta_m &\approx \arg\left(\Delta r - j \frac{\Delta\theta}{2} \sinh(2r)\right) + \Delta\theta \sinh^2 r. \end{aligned} \quad (19)$$

It is worth highlighting the asymmetric sensitivity revealed by Eq. (19): the total residual squeezing r_m is significantly more sensitive to the phase mismatch $\Delta\theta$ than to the magnitude mismatch Δr . This arises because the phase mismatch term is scaled by the coefficient $\frac{1}{2} \sinh(2r)$, which grows rapidly with the squeezing parameter r (and thus the signal energy N). This leads to a ‘‘dominant masking effect’’: in the presence of non-negligible phase mismatch, its contribution to r_m typically far exceeds that of the magnitude mismatch. Given the geometric relationship $r_m \approx \sqrt{(\Delta r)^2 + (K\Delta\theta)^2}$, the value of r_m becomes almost entirely determined by the phase mismatch term. This explains the phenomenon observed in the simulation results (see Fig. 2(a) and (b)), where the error probability curves for $(\Delta r, \Delta\theta) = (0.00, 0.03\pi)$ and $(0.02, 0.03\pi)$ nearly coincide. Consequently, in experimental systems, the requirement for phase locking precision is much more stringent than that for amplitude matching.

Phase-only mismatch ($\Delta r = 0$):

$$\begin{aligned} r_m &\approx \frac{|\Delta\theta|}{2} \sinh(2r) = |\Delta\theta| \frac{N(N+1)}{2N+1}, \\ \theta_m &\approx -\frac{\pi}{2} \text{sgn}(\Delta\theta) + \Delta\theta \sinh^2 r = -\frac{\pi}{2} \text{sgn}(\Delta\theta) + \Delta\theta \frac{N^2}{2N+1}, \pmod{2\pi}. \end{aligned} \quad (20)$$

Amplitude-only mismatch ($\Delta\theta = 0$):

$$r_m \approx |\Delta r|, \quad \theta_m \approx \begin{cases} 0, & \Delta r > 0, \\ \pi, & \Delta r < 0, \end{cases} \pmod{2\pi}. \quad (21)$$

We now calculate the photon number probability distribution of ζ_i^{sm} . Ignoring the rotation $R(\vartheta)$ which does not affect photon statistics, the equivalent output states derived from Eq. (15) are:

$$\zeta_0^{\text{sm}} \sim S(z_m) |0\rangle, \quad \zeta_1^{\text{sm}} \sim S(z_m) |2\gamma\rangle. \quad (22)$$

To utilize standard photon number distribution formulas, we rewrite ζ_1^{sm} as a displaced squeezed vacuum state:

$$\zeta_1^{\text{sm}} \sim S(z_m) |2\gamma\rangle = D(2\gamma_m) S(z_m) |0\rangle, \quad (23)$$

where

$$\gamma_m = \gamma \cosh r_m + \gamma^* e^{i\theta_m} \sinh r_m. \quad (24)$$

Consequently, the Poissonian distribution valid for the ideal IS-Kennedy (Eq. (8)) no longer applies. For an ideal PNR(M) detector (considering only finite resolution), the probability of detecting n photons given hypotheses i is:

$$P(n|i) = \text{Tr}(\Pi_n \zeta_i^{\text{sm}}) = \begin{cases} p_n^{\text{sv}}(r_m), & i = 0, \\ p_n^{\text{dss}}(2\gamma_m, r_m, \theta_m), & i = 1, \end{cases} \quad (25)$$

where the corresponding distribution is used for $n \leq M-1$, and the truncation/saturation bin is defined as $P(n = M|i) = 1 - \sum_{n=0}^{M-1} P(n|i)$. Here, $p_n^{\text{sv}}(r_m)$ denotes the photon number distribution of the squeezed vacuum state (Eq. (A2)), and $p_n^{\text{dss}}(2\gamma_m, r_m, \theta_m)$ denotes that of the displaced squeezed vacuum state (Eq. (A4)).

The introduction of mismatch results in ζ_0^{sm} becoming a squeezed vacuum state (containing only even photon numbers), while ζ_1^{sm} becomes a displaced squeezed vacuum state whose Fock distribution generally exhibits even-odd oscillations (see Fig. 2(d)). This implies that the likelihood function $L(n)$ does not necessarily vary monotonically with the photon number n . Consequently, the MAP decision generally becomes a set-based decision (potentially involving a multi-threshold structure) rather than a simple single-threshold test. Therefore, the minimum error probability (Eq. (11)) is reformulated as:

$$P_{\text{err}}^{\text{ISK,sm}} = 1 - \frac{1}{2} \sum_{n=0}^M \max\{P(n|i=0), P(n|i=1)\}. \quad (26)$$

When employing an SPD, the observation yields only two outcomes: $n = 0$ (no-click) and $n \geq 1$ (click). Under equal priors, the MAP decision is equivalent to a binary mapping of these outcomes. Since $P(0|0) \geq P(0|1)$ (as the exponent in the latter is ≤ 0), the MAP rule maps to on-off detection: click decides hypotheses 1, no-click decides hypotheses 0. The false alarm probability is:

$$P_{\text{FA}} = P(\text{click}|0) = 1 - P(n=0|i=0) = 1 - \frac{1}{\cosh r_m}. \quad (27)$$

The miss detection probability is:

$$P_{\text{M}} = P(n=0|i=1) = \frac{1}{\cosh r_m} \exp(-|2\gamma_m|^2 + \text{Re}[e^{-i\theta_m}(2\gamma_m)^2] \tanh r_m). \quad (28)$$

These equations clearly reveal that the residual squeezing r_m reduces the vacuum component of ζ_0^{sm} , thereby increasing the false alarm probability, while θ_m modifies the vacuum overlap of ζ_1^{sm} through the exponential term.

Furthermore, we consider the saturation characteristics in the case of amplitude-only mismatch ($\Delta r \neq 0, \Delta\theta = 0$). As the signal energy tends to infinity ($N \rightarrow \infty$), the mean photon number of the signal state ζ_1^{sm} far exceeds the resolution M of the PNR detector, leading to $P_{\text{Mi}} \rightarrow 0$. In this regime, the error probability of the IS-Kennedy is dominated by the false alarm probability. The MAP strategy is thus equivalent to a threshold decision with $n_{\text{th}}^* = M$: decide hypotheses 1 if the outcome falls into the saturation bin $n = M$, and hypotheses 0 otherwise. Since ζ_0^{sm} is a squeezed vacuum state with a non-zero photon number distribution only for even terms (see Eq. (A2)), the saturation error probability is:

$$P_{\text{sat}} \approx \frac{1}{2} P_{\text{FA}} = \frac{1}{2} \sum_{k=\lceil M/2 \rceil}^{\infty} p_{2k}^{\text{sv}}(r_m) = \frac{1}{2} \sum_{k=\lceil M/2 \rceil}^{\infty} \frac{(2k)!}{2^{2k}(k!)^2} \frac{\tanh^{2k}(r_m)}{\cosh(r_m)}. \quad (29)$$

Under the condition of small mismatch ($\Delta r \ll 1$), we have $|\Delta r| = r_m$ and $\tanh r_m \approx r_m = |\Delta r|$, and the summation is dominated by the first term. Letting $n_{\text{min}} = 2 \lceil \frac{M}{2} \rceil$, the error probability simplifies to:

$$P_{\text{sat}} \approx \frac{1}{2} p_{n_{\text{min}}}^{\text{sv}}(r_m) = \frac{1}{2} \frac{n_{\text{min}}!}{2^{n_{\text{min}}} [(n_{\text{min}}/2)!]^2} (\Delta r)^{n_{\text{min}}}. \quad (30)$$

This equation reveals the ‘‘parity step effect’’ of the PNR detector in resisting mismatch: increasing the detector resolution M does not continuously reduce the saturation error probability. Instead, the order of magnitude of the error probability transitions only when M crosses an even integer threshold. Substituting $M = 1$ and $M = 3$ confirms that the calculated results are consistent with the simulation results (see Fig. 2(a) and (b)).

III. SIMULATION METHODS AND RESULTS

The numerical results were obtained using QuTiP in Python [8]. We model the receiver output states in a truncated Fock space and compute the photon-number distributions from the corresponding density operators. Unless otherwise specified, the simulations use a cutoff $N_{\text{cut}} = 100$. We verified numerical convergence by increasing the cutoff dimension until the resulting error probabilities changed negligibly. For each mean photon number N , the S-BPSK states were generated with the optimal squeezing fraction $\beta_{\text{opt}} = \frac{N}{2N+1}$.

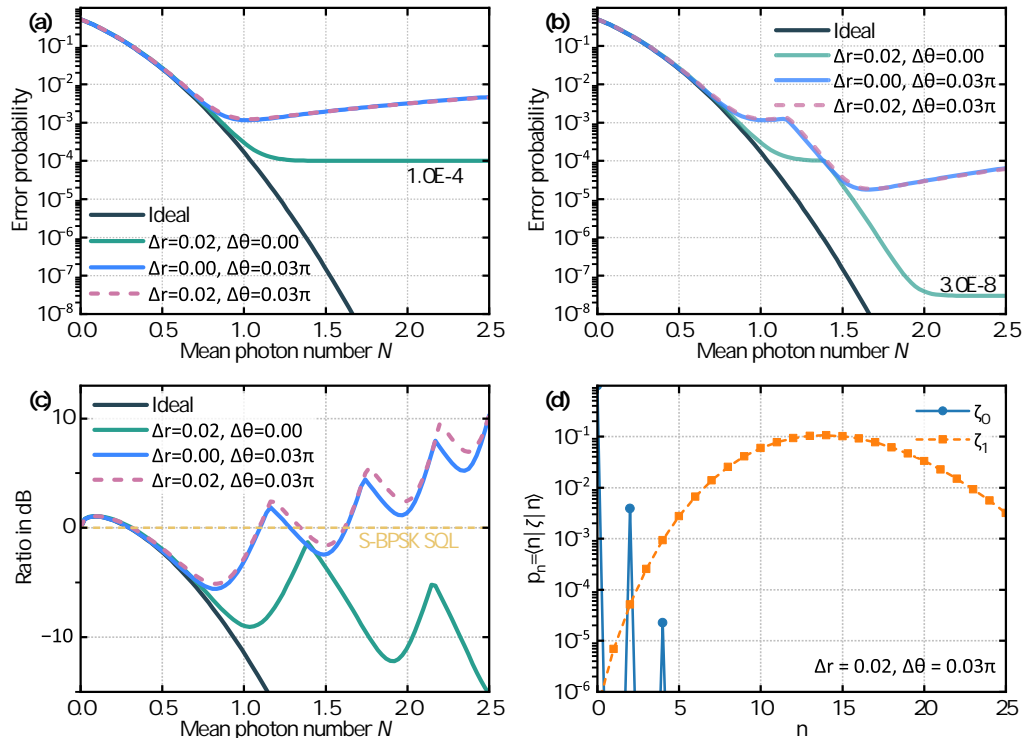


FIG. 2. Performance analysis of the IS-Kennedy receiver under inverse-squeezing mismatch conditions. (a) Error probability of IS-Kennedy with SPD. (b) Error probability of IS-Kennedy with PNR(3). (c) The performance ratio (in dB) of IS-Kennedy with PNR(10) relative to the S-BPSK SQL. (d) The Fock-basis population of $\zeta_0^{\text{sm}}, \zeta_1^{\text{sm}}$ with inverse-squeezing mismatch of $\Delta r = 0.02, \Delta\theta = 0.03\pi$.

Figure 2(a) and Fig. 2(b) show the error probability under SPD and PNR(3), respectively. In the ideal case, the error decreases rapidly with N , reflecting the benefit of the inverse-squeezing transformation. Under amplitude-only mismatch, $(\Delta r, \Delta\theta) = (0.02, 0)$, the performance remains close to the ideal curve at low N but saturates at high N , as expected from the residual squeezing acting on the nulled state ζ_0^{sm} . The saturation levels agree with Eq. (30): for SPD the error floor is about 10^{-4} , whereas for PNR(3) it is reduced to about 3×10^{-8} . This confirms the parity-step behavior predicted by the small-mismatch analysis, namely that increasing the PNR resolution suppresses the amplitude-mismatch-induced error only when the resolution crosses an even-photon threshold. The physical origin is illustrated in Fig. 2(d): under mismatch, ζ_0^{sm} becomes a squeezed vacuum with only even-photon components. As a result, the likelihood function is generally non-monotonic in photon number, and the MAP decision is no longer a simple single-threshold rule.

Phase mismatch causes a much stronger degradation. For $(\Delta r, \Delta\theta) = (0, 0.03\pi)$, the error begins to deviate from the ideal case at moderate N and increases significantly at higher energies. Moreover, the curves for $(0, 0.03\pi)$ and $(0.02, 0.03\pi)$ nearly overlap in both Fig. 2(a) and Fig. 2(b), showing that once phase mismatch is present, the additional effect of amplitude mismatch is comparatively weak. This is consistent with Eq. (19), where the phase-mismatch contribution is amplified by $\sinh(2r)/2$ and therefore dominates the residual squeezing strength r_m at sufficiently large squeezing (i.e. at high N). Although finite-resolution PNR clearly outperforms SPD in the mismatched regime, it does not remove the dominant sensitivity to phase mismatch.

Figure 2(c) further plots the error-probability ratio in dB relative to the S-BPSK SQL, where negative values indicate performance below the SQL. In the ideal case, the IS-Kennedy receiver preserves a clear advantage as N increases. Under amplitude-only mismatch, this advantage is largely maintained over a broad range of N , but is

eventually limited by the saturation effect. By contrast, phase mismatch rapidly reduces the SQL advantage, and the error probability even continues to rise at large N .

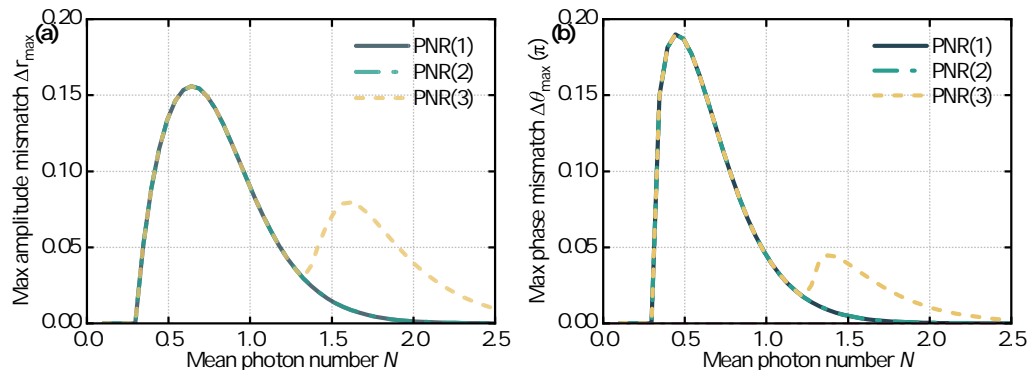


FIG. 3. The maximum tolerable inverse-squeezing mismatch for which the IS-Kennedy receiver still outperforms the S-BPSK SQL, i.e., $P_{\text{err}}^{\text{ISK}} < P_{\text{SQL}}^{\text{S-BPSK}}$. (a) Maximum tolerable amplitude mismatch Δr_{\max} versus mean photon number N . (b) Maximum tolerable phase mismatch $\Delta \theta_{\max}$ versus N . Results are shown for PNR(1), PNR(2), and PNR(3).

Figure 3 provides a more direct robustness metric by showing the maximum tolerable inverse-squeezing mismatch for which the IS-Kennedy receiver still outperforms the S-BPSK SQL, i.e., $P_{\text{err}}^{\text{ISK}} < P_{\text{SQL}}^{\text{S-BPSK}}$. As shown in Fig. 3(a), the tolerable amplitude mismatch Δr_{\max} is non-monotonic in N : it first increases, reaches its largest value in the low-to-intermediate energy region, and then decreases at higher N . For PNR(1) and PNR(2), the admissible range rapidly shrinks at large N , whereas PNR(3) retains an additional tolerance window. A similar trend is observed for the phase mismatch in Fig. 3(b), but the tolerable phase error collapses more rapidly with increasing N , in agreement with the enhanced phase sensitivity predicted by Eq. (19). Moreover, the extra tolerance window preserved by PNR(3) is consistent with the parity-step behavior discussed above: increasing the PNR resolution improves mismatch robustness in a non-smooth, threshold-like manner rather than continuously.

Overall, the simulations show that the IS-Kennedy receiver is far more sensitive to phase mismatch than to amplitude mismatch, and that finite-resolution PNR improves robustness mainly against amplitude mismatch rather than imperfect phase locking.

IV. CONCLUSION

In conclusion, we have investigated inverse-squeezing mismatch in the IS-Kennedy receiver for the discrimination of binary displaced squeezed vacuum states. We showed that imperfect inverse squeezing is equivalent to a residual squeezing after nulling, which modifies the output photon-number statistics and makes the optimal MAP decision generally non-single-threshold. The analysis further reveals a strong asymmetry between the two mismatch types: the receiver is much more sensitive to phase mismatch than to amplitude mismatch, because the phase error is effectively amplified by the squeezing process. Numerical results confirm that amplitude-only mismatch leads to a saturation error floor, and that finite-resolution PNR detection suppresses this floor in a parity-step manner rather than continuously with detector resolution. By contrast, phase mismatch rapidly degrades the receiver performance and can destroy its advantage over the S-BPSK SQL at high signal energies. The maximum-tolerable-mismatch results further show that the practically useful operating region of the IS-Kennedy receiver is ultimately limited by phase locking. These results clarify the physical origin of mismatch-induced degradation and provide guidance for the experimental design of inverse-squeezing receivers with finite-resolution photon counting.

Appendix A: Fock-basis Population of Squeezed Vacuum and Displaced Squeezed States

Let the Squeezed Vacuum (SV) state and the Displaced Squeezed State (DSS) be denoted, respectively, as:

$$S(z)|0\rangle \quad \text{and} \quad D(\alpha)S(z)|0\rangle, \quad (\text{A1})$$

where the squeezing parameter is complex, $z = re^{j\theta}$ (with $j = \sqrt{-1}$).

The photon number distribution of the Squeezed Vacuum (SV) state is non-zero only for even photon numbers:

$$p_{2k}^{\text{sv}}(r) = \frac{(2k)! \tanh^{2k}(r)}{2^{2k}(k!)^2 \cosh(r)}, \quad (\text{A2})$$

$$p_{2k+1}^{\text{sv}}(r) = 0. \quad (\text{A3})$$

The photon number distribution of the Displaced Squeezed State (DSS) can be expressed in terms of Hermite polynomials, $H_n(\cdot)$:

$$p_n^{\text{dss}} = \frac{1}{n! \cosh r} \left(\frac{\tanh r}{2} \right)^n \left| H_n \left(\frac{\alpha e^{-j\theta/2}}{\sqrt{\sinh r \cosh r}} \right) \right|^2 \exp(-|\alpha|^2 + \text{Re}[e^{-j\theta} \alpha^2] \tanh r). \quad (\text{A4})$$

ACKNOWLEDGMENTS

This work was supported by Independent Innovation Science Fund Program of National University of Defense Technology, China (Grant No. 22-ZZCX-036), Key research & development program of Guangxi (Grant No. GuiKeAB23075155), Innovative Talent Development Fund of Information Support Force Engineering University (Grant No. XJKT-QT-25-02-GW), and the Key Research & Development Program of Guangxi (Grant No. AB23075112).

DATA AVAILABILITY

The data that support the findings of this study are available from the authors upon request.

CODE AVAILABILITY

The numerical simulations in this study were performed in Python using QuTiP 5.1.1. The custom scripts used to generate the results are available from the corresponding author on reasonable request.

COMPETING INTERESTS

The authors declare no competing interests.

-
- [1] E. Bai, J. Peng, T. Wu, K. Wen, F. Sun, C. Zhou, Y. Li, Z. Zhang, and C. Dong, [Near-optimal discrimination of displaced squeezed binary signals using displacement, inverse-squeezing, and photon-number-resolving detection](#) (2026), [arXiv:2601.09073 \[quant-ph\]](#).
- [2] M. G. A. Paris, Nearly ideal binary communication in squeezed channels, *Phys. Rev. A* **64**, 014304 (2001).
- [3] G. Chesi, S. Olivares, and M. G. A. Paris, Squeezing-enhanced phase-shift-keyed binary communication in noisy channels, *Phys. Rev. A* **97**, 032315 (2018).
- [4] A. Walsh, L. Conlon, B. Shajilal, O. Erkilic, J. Janousek, S. Assad, J. Zhao, and P. K. Lam, [All-gaussian state discrimination beyond the coherent helstrom bound](#) (2025), [arXiv:2510.20096 \[quant-ph\]](#).
- [5] D. Ganapathy, W. Jia, and M. Nakano (LIGO O4 Detector Collaboration), Broadband quantum enhancement of the ligo detectors with frequency-dependent squeezing, *Phys. Rev. X* **13**, 041021 (2023).
- [6] L. Gao, S. Shi, B. Lu, L.-A. Zheng, L. Tian, W. Li, Y. Wang, and Y. Zheng, Generating long-term stable squeezed states via multiple pump noise suppression, *Opt. Lett.* **50**, 4674 (2025).
- [7] R. S. Kennedy, A near-optimum receiver for the binary coherent state quantum channel, Research Laboratory of Electronics, MIT, Quarterly Progress Report **108**, 219 (1973).
- [8] N. Lambert, E. Giguère, P. Menczel, B. Li, P. Hopf, G. Su'arez, M. Gali, J. Lishman, R. Gadhvi, R. Agarwal, A. Galicia, N. Shammah, P. Nation, J. R. Johansson, S. Ahmed, S. Cross, A. Pitchford, and F. Nori, Qutip 5: The quantum toolbox in Python, *Phys. Rep.* **1153**, 1 (2026).